Combining CXCR4-targeted and nontargeted nanoparticles for effective unassisted in vitro magnetic hyperthermia

Vânia Vilas-Boas, Begoña Espiña, Yury V. Kolen'ko, Manuel Bañobre-Lopez, José A. Duarte, Verónica C. Martins, Dmitri Y. Petrovykh, Paulo P. Freitas, and Felix D. Carvalho

Citation: Biointerphases **13**, 011005 (2018);
View online: https://doi.org/10.1116/1.5009989
View Table of Contents: http://avs.scitation.org/toc/bip/13/1
Published by the American Vacuum Society

Combining CXCR4-targeted and nontargeted nanoparticles for effective unassisted *in vitro* magnetic hyperthermia

Vânia Vilas-Boas[a)]
UCIBIO-REQUIMTE, Laboratory of Toxicology, Biological Sciences Department, Faculty of Pharmacy, University of Porto, Rua de Jorge Viterbo Ferreira, 228, 4050–313 Porto, Portugal and International Iberian Nanotechnology Laboratory, Av. Mestre José Veiga, 4715-330 Braga, Portugal

Begoña Espiña, Yury V. Kolen'ko, and Manuel Bañobre-Lopez
International Iberian Nanotechnology Laboratory, Av. Mestre José Veiga, 4715-330 Braga, Portugal

José A. Duarte
CIAFEL, Faculty of Sports, University of Porto, Rua Dr. Plácido da Costa 91, 4200-450 Porto, Portugal

Verónica C. Martins,[b)] Dmitri Y. Petrovykh,[c)] and Paulo P. Freitas
International Iberian Nanotechnology Laboratory, Av. Mestre José Veiga, 4715-330 Braga, Portugal

Felix D. Carvalho[d)]
UCIBIO-REQUIMTE, Laboratory of Toxicology, Biological Sciences Department, Faculty of Pharmacy, University of Porto, Rua de Jorge Viterbo Ferreira, 228, 4050–313 Porto, Portugal

(Received 21 October 2017; accepted 25 January 2018; published 5 February 2018)

The use of targeted nanoparticles for magnetic hyperthermia (MHT) increases MHT selectivity, but often at the expense of its effectiveness. Consequently, targeted MHT is typically used in combination with other treatment modalities. This work describes an implementation of a highly effective monotherapeutic *in vitro* MHT treatment based on two populations of magnetic particles. Cells were sequentially incubated with two populations of magnetic particles: nonfunctionalized superparamagnetic nanoparticles and anti-CXCR4-functionalized particles. After removing the excess of free particles, an alternating magnetic field (AMF) was applied to produce MHT. The induced cytotoxicity was assessed at different time-points after AMF application. Complete loss of cell viability was observed 72 h after MHT when the iron loading of the anti-CXCR4-functionalized particles was boosted by that of a nontargeted population. Additionally, induction of necrosis resulted in more efficient cell death than did induction of apoptosis. Achieving a uniquely high effectiveness in monotherapeutic MHT demonstrates the potential of this approach to achieve complete loss of viability of cancer cells while avoiding the side effects of dual-treatment strategies that use MHT only as a sensitizing therapy. *Published by the AVS*. https://doi.org/10.1116/1.5009989

I. INTRODUCTION

Heat production by magnetic nanoparticles (MNPs) exposed to an alternating magnetic field (AMF), denoted magnetic hyperthermia (MHT), has been explored as a cancer treatment,[1] whereby tumor cell death is induced by apoptosis or necrosis, depending on the temperatures reached during the MHT.[2] Gordon was the first to use magnetic fluids for the purpose of inducing MHT to treat tumors in rats, having described the occurrence of "intracellular hyperthermia," inferring that cell membranes acted as insulators that prevented heat dissipation to other cells.[3] This revolutionary concept implied that exposing a single cell loaded with nanoparticles to an AMF would result in cell death.

Subsequent MHT studies, however, revealed practical limitations of the intracellular concept. For example, theoretical calculations by Rabin[4] concluded that at least 200 000 cells loaded with 500 pg of iron would be necessary to induce hyperthermic conditions, thus suggesting that the intracellular concept had no biophysical basis. Most of the reports in the literature thereafter followed Rabin's predictions and considered volumetric MHT, i.e., the application of an AMF of a mixture of cells with MNPs (internalized or not) that results in a volumetric temperature increase, ultimately leading to a cytotoxic effect.[5–8] Depending on the temperature, the cytotoxic effect could result in cell death by either apoptosis or necrosis.[2]

Targeting strategies with nanoparticles functionalized with antibodies,[9] peptides,[5,8,10] or other biomolecules[6,7] have been proposed to enhance the *selectivity* of MHT for cancer cells, i.e., attempting to restrict the MHT-induced cytotoxicity to cancer cells. Most studies so far, however, report that targeted MHT fails to reach a 100% lethal outcome for the treated cancer cells, thus exhibiting limited *effectiveness*. The apparent practical limit on the effectiveness of targeted MHT is encountered despite highly efficient targeting, whether evaluated by the fraction of retained particles or by the concentration of particles associated with individual targeted cells. Accordingly, MHT has been typically used in combination with other therapies,[11–15] including stereotactic radiotherapy,[16] or anticancer drugs,[17–19] in an attempt to improve the overall treatment effectiveness.

[a)]Electronic mail: vvilasboas@ff.up.pt
[b)]Present address: INESC–Microsistemas e Nanotecnologias, Rua Alves Redol 9, Lisbon 1000-029, Portugal.
[c)]Electronic mail: dmitri.petrovykh@inl.int
[d)]Electronic mail: felixdc@ff.up.pt

We hypothesize that instead of using MHT only as a supplement for other therapies, it may be possible to enhance the effectiveness of a "pure" MHT strategy by further increasing the total iron loading, which would increase the temperature achieved during MHT and result in 100% lethal outcome for cancer cells in the targeted volume. Given the apparent limit on iron loading that can be achieved using a single population of targeted (specific) particles, we propose to augment the iron loading by adding a second nontargeted (nonspecific) particle population. As a proof of principle, this work demonstrates *in vitro* a therapeutic strategy based on the combined use of both CXCR4-targeted (specific) and nontargeted (nonspecific) magnetic nanoparticles to produce cytotoxic magnetic hyperthermia in model cancer cells in a monotherapeutic context, by ensuring that lethal temperatures are reached under an AMF.

II. EXPERIMENT

A. Chemicals and reagents

All reagents used in this study were of analytical grade or of the highest grade available. Fetal bovine serum (FBS) was purchased from HyClone UK, Ltd., Northumberland, England, UK. Penicillin ($10\,000\,\mathrm{U\,ml^{-1}}$) and streptomycin ($10\,000\,\mu\mathrm{g\,ml^{-1}}$), herein referred to as Pen-Strep, Roswell Park Memorial Institute (RPMI-1640) cell culture medium, sodium pyruvate, nicotinamide adenine dinucleotide reduced form (NADH), triton X-100, caspase-3 fluorimetric substrate *N*-acetyl-Asp-Glu-Val-Asp-7-amido-4-methylcoumarin (Ac-DEVD-AMC), 4-(2-hydroxyethyl)piperazine-1-ethanesulfonic acid (HEPES), 3-[(3-cholamidopropyl)dimethylammonio]-1-propane-sulfonate hydrate (CHAPS), dithiothreitol (DTT), ethylenediaminetetraacetic acid (EDTA), KH_2PO_4, $K_2HPO_4 \cdot 3H_2O$, $CaCl_2$, NaCl, glycerol, staurosporine (STS) from *Streptomyces* sp., propidium iodide (Pi), glutaraldehyde solution (25% in water), hydrochloric acid, sodium cacodylate trihydrate, calcein-AM solution, and bovine serum albumin (BSA) were purchased from Sigma-Aldrich, Inc. (St. Louis, MO). Antihuman CXCR4, clone 12G5, low endotoxin, azide-free monoclonal antibody produced in mouse, and its matched isotype-control, mouse antihuman monoclonal IgG2a, were purchased from BioLegend Inc. (San Diego, CA).

B. Cell culture

Human acute T-cell leukemia cell line Jurkat (JK), clone E6.1 (ATCC® TIB-152™), was purchased from the American Type Culture Collection (Manassas, VA). This cell line was grown in RPMI-1640 medium supplemented with 10% FBS, 1% Pen-Strep and maintained in a controlled atmosphere at 37 °C and 5% CO_2.

C. CXCR4 expression in Jurkat cells

Surface expression of CXCR4 receptor in JK cells was assessed by flow cytometry after incubating ca. 5×10^5 cells with 2 μl mouse antihuman monoclonal CXCR4 antibody (clone 12G5, BioLegend, Inc., San Diego, CA) for 1 h, at 37 °C, in the dark, in 2% BSA in Hanks balanced salt solution with calcium and magnesium salts (HBSS +/+). In parallel, samples with the matched isotype control (IC) antibody (mouse antihuman monoclonal IgG2a, BioLegend, Inc., San Diego, CA) were prepared to depict unspecific staining. Cells were then washed with cold phosphate-buffered saline (PBS) and further incubated with atto-633 labeled antimouse antibody produced in goat (Sigma-Aldrich, Inc., St. Louis, MO) for 30 min, at 37 °C. After this incubation period, cells were washed again with PBS and kept on ice, in the dark, until flow cytometry analysis. The expression of that receptor was also assessed in normal cells using peripheral blood mononuclear cells (PBMC), which were isolated from whole blood using a previously established protocol[20] described in detail in the supplementary material.[42]

D. Incubation of cells with nanoparticles for *in vitro* magnetic hyperthermia

Poly(acrylic acid)-coated magnetic nanoparticles (SPION), with an average iron-oxide core diameter of 17.9 ± 4.4 nm (from transmission electron microscopy, TEM) have been previously synthesized and extensively characterized.[21] Two million cells per test condition were resuspended in 1 ml of a $0.362\ \mathrm{g_{Fe}\,l^{-1}}$ SPION suspension in cell culture medium (final sample volume 1 ml), for 2 h, with mild agitation. Samples were then centrifuged at 125*g* for 5 min, the supernatant was discarded, and the pellet was resuspended in a $0.396\ \mathrm{g_{Fe}\,l^{-1}}$ suspension of dextran-coated 250 nm magnetic particles (MP) (09-20-252 Nanomag®-D, Micromod Partikeltechnologie GmbH, Rostock, Germany), in 2% BSA in HBSS +/+, for 1 h, at 37 °C, with mild agitation (final sample volume 1 ml). These particles have covalently bound protein-A at their surface and were previously incubated with CXCR4 or IC antibodies, for 1 h, at 37 °C, with agitation, to obtain functionalized particles (MP–CXCR4 or MP–IC, respectively). Samples were then centrifuged at 125*g* for 5 min, washed with cell culture medium, centrifuged again, recovered in 1 ml cell culture medium, and transferred to glass vials, previously blocked with BSA, for the magnetic hyperthermia experiments. Incubation of cells with only SPION (2 h, 37 °C, in cell culture medium) or only MP–CXCR4 (1 h, 37 °C, in 2% BSA in HBSS +/+) was also performed.

E. MHT treatment

The application of the AMF to the samples described in Sec. II D was performed using a magnetic field generator (DM 100, nB nanoScale Biomagnetics, Zaragoza, Spain) operating at 869 kHz and $20\ \mathrm{kA\,m^{-1}}$ for 30 min, followed by another 30 min at 554 kHz and $24\ \mathrm{kA\,m^{-1}}$. The temperature of the suspension was measured using an optical temperature probe included in the equipment and the average constant temperature reached in the second step of AMF was denoted as *T*c. After AMF application, cells were seeded and subsequently tested to determine the levels of MHT-induced cytotoxicity at successive points in time.

F. SAR measurements

For specific absorption rate (SAR) determination, temperature increases of suspensions of only SPIONs (0.362 $g_{Fe}\,l^{-1}$) or only MPs (0.265 $g_{Fe}\,l^{-1}$) in cell culture medium were recorded during a 10 min application of an AMF (869 kHz; 20 kA m^{-1}). A sample of only cell culture medium was also run under the same AMF conditions (blank), to discriminate the effect of the MNP-induced heating and the increase in temperature arising from the heating of the coil.[22] SAR values for each type of nanoparticles were calculated using the following equation:

$$\mathrm{SAR}\left(\frac{W}{g}\right) = \frac{C}{m_{\mathrm{Fe}}} \times \frac{dT_{\mathrm{sample}} - dT_{\mathrm{blank}}}{dt},$$

where C is the heating capacity of water (4.186 J $g^{-1}\,°C^{-1}$), m_{Fe} is the mass of iron per unit volume of sample, and $dT_{sample} - dT_{blank}/dt$ is the variation in the sample temperature, during the 10 min exposure to AMF, with the increase in temperature observed in the cell culture medium alone (blank) subtracted as a baseline.

G. TEM for SPION uptake studies

Samples were prepared following a previously established protocol.[23] Briefly, JK cells with SPIONs were pelleted at 300g for 5 min, fixed with 2.5% glutaraldehyde in 0.1 M sodium cacodylate buffer pH 7.4, for 2 h, and rinsed with cacodylate buffer 0.1 M. Samples were then postfixed in 2% osmium tetroxide, dehydrated with graded ethanol, embedded in Epon, and stored for 2–3 days at 60 °C to promote resin polymerization. Ultrathin (100 nm) sections, contrasted with uranylacetate and lead citrate, were then prepared on copper grids (300 Mesh) for TEM analysis (Zeiss EM10A, Carl Zeiss, Oberkochen, Germany). We note that in contrast with SPION-incubated cells, the large size of MP–CXCR4 and MP–IC particles (ca. 250 nm) makes MP-incubated cells not readily compatible with microtome preparation as 100-nm ultrathin sections.

H. Confirming specific (targeted) interactions

Cells were incubated with MP–CXCR4 or MP–IC (1 h, 37 °C, in 2% BSA in HBSS +/+) and, after removing the excess of free particles by centrifugation (125g, 5 min), samples were incubated with atto-633 labeled antimouse antibody produced in goat (Sigma-Aldrich, Inc., St. Louis, MO), for 30 min, at 37 °C. Samples were further incubated with 0.4 μM, for flow cytometry studies, or 1 μM calcein-AM and then seeded in 8-well μ-slide (Ibidi, Martinsried, Germany) for laser scanning confocal microscopy (LSCM) using a Zeiss LSM780 confocal microscope. Isolation of PBMC was performed as described in the supplementary material.[42] For flow cytometry studies, a S3™ cell sorter (Bio-Rad Laboratories, Hercules, CA), equipped with 488 and 561 nm lasers, was used as a flow cytometer to acquire the fluorescence signals in logarithmic mode. JK cell population was defined setting a polygon gate according to their light scattering properties (forward versus side scatter plot) excluding cell debris. Fluorescence due to calcein was followed in FL-1 channel, and atto-633 fluorescence was collected in FL-4. Flow-cytometry-standard files were analyzed using FlowJo® v.10.1 software (FlowJo LCC, Ashland, OR).

I. Iron quantification by inductively coupled plasma–optical emission spectroscopy

Cells were incubated with SPION only, MP–CXCR4 only, SPION+MP–CXCR4, or SPION+MP–IC following the procedure described in Sec. II D. For the inductively coupled plasma-optical emission spectroscopy (ICP-OES) measurements, samples were digested with 1 ml concentrated hydrochloric acid for 24 h and then diluted with ultrapure water (Milli-Q®, Merck Millipore) to a final volume of 50 ml. Measurements were performed in triplicates, in an ICPE-9000 Multitype ICP Emission Spectrometer (Shimadzu).

J. Assessment of MHT-induced cytotoxicity

All the following experiments include the anticancer drug STS (2.5 μM, 1 h exposure) as a positive control for apoptotic cell death.

1. Annexin-V and propidium iodide labeling for flow cytometry

The translocation of phosphatidylserine residues from the inner to the outer leaflet of the cell membrane is considered one of the earliest events of apoptosis.[24] A previously described protocol[25] was used with minor modifications. Briefly, 2 h after MHT, 2×10^5 cells were collected in cell culture medium, washed with PBS, and resuspended in 200 μl of Annexin-V binding buffer (diluted from the 10× stock solution: 0.1 M HEPES, pH 7.4; 1.4 M NaCl; 25 mM $CaCl_2$) in 2% BSA, with or without 5 μl of BD Pharmingen™ FITC labeled Annexin-V (AnV–FITC; BD Biosciences), and kept for 20 min, at room temperature, in the dark. Cells were centrifuged at 210g, 5 min, at 4 °C, and immediately analyzed; Pi (5 μg ml^{-1}) was used to detect membrane damage in these samples.

Flow cytometry parameters were set as described in Sec. II H, using positive and negative controls. Fluorescence collected in FL-1 channel (green fluorescence from AnV–FITC) was plotted versus the one collected in FL-3 channel (red fluorescence from Pi), and the percentage of positive cells for each channel (or both) estimated after establishing the quadrants based on the controls. For each sample, at least 1.5×10^4 gated events were counted and distinguished as living cells (AnV–$FITC^-$/Pi^-, lower left quadrant); apoptotic cells (AnV–$FITC^+$/Pi^-, upper left quadrant); late stage apoptosis or necrotic cells (AnV–$FITC^+$/Pi^+, upper right quadrant), and necrotic cells (AnV–$FITC^-$/Pi^+, lower right quadrant). The percentage of dying cells corresponds to the sum of all the labeled events.

2. Caspase-3 activity assay

After MHT, at least 1×10^6 cells per well were seeded in six-well plates and maintained in a controlled atmosphere at 37 °C and 5% CO_2 for 24 h. Cells were then collected on ice, centrifuged at 850*g*, for 5 min, at 4 °C, washed with PBS and resuspended in 35 μl of a lysis buffer (50 mM HEPES, 0.1 mM EDTA, 1.63 mM CHAPS supplemented with 1 mM DTT before using). After vigorous vortexing, the samples were kept at −80 °C until analysis.

On the day of analysis, samples were thawed on ice, vortexed, and left to equilibrate for 10 min on ice before centrifugation at 16 000*g*, for 10 min, at 4 °C. The supernatant was collected to new tubes, and the pellet was discarded. For each assay, 10 μl of this supernatant were mixed with 90 μl of an assay buffer (50 mM HEPES, 100 mM NaCl, 1 mM EDTA, 1.63 mM CHAPS, and 10% glycerol supplemented with 10 mM DTT before using), containing 14.8 μM fluorimetric substrate (Ac-DEVD-AMC), and the kinetic reading was immediately started. A Synergy H1 microplate reader (BioTek Instruments, Bad Friedrichshall, Germany) was used to perform the kinetic readings (at 37 °C; excitation at 380 nm, emission at 460 nm), which lasted for 3 h with successive readings at each 10 min. The amount of protein loaded per well was estimated using Coomassie Plus (Bradford) Protein kit (Thermo Fisher Scientific, Inc., Rockford, IL) following the manufacturer's instructions. Caspase-3 activity was expressed as the slope of the curve obtained plotting the protein corrected-fluorescence signals versus time (RFU μg^{-1} min^{-1}).

3. Metabolic rate assay

After MHT, cells were seeded in 96-well plates (15 000 cells per well) and maintained in a controlled atmosphere (37 °C, 5% CO_2) until cell viability was assessed 24 and 72 h after AMF application. For that purpose, 10 μl PrestoBlue® cell viability reagent (Molecular Probes™, Carlsbad, CA) was added to each well. After incubation at 37 °C for 3 h, the conversion of resazurin to resorufin by viable cells was tracked by collecting the fluorescence signals using a microplate reader (Synergy H1, BioTek Instruments) with excitation wavelength at 560 nm and emission wavelength at 590 nm.

4. Lactate dehydrogenase leakage assay

Lactate dehydrogenase (LDH) activity in the cell culture medium was assessed spectrophotometrically following the decrease in absorbance of NADH during the reduction of pyruvate to lactate, as an indicator of membrane disruption, i.e., cell death. A previously described protocol[26] was used with minor modifications.

Briefly, after MHT, 2×10^4 cells per well were seeded in 96-well plates and maintained in a controlled atmosphere (37 °C, 5% CO_2) until LDH leakage was assessed 24 and 72 h after AMF application. From each well, 50 μl of cell culture medium were collected (to measure extracellular LDH content) and replaced by 50 μl of a 0.5% Triton X-100 solution in cell culture medium (to induce cell lysis). After incubating for 1 h, at 37 °C, 25 μl of cell culture medium were collected to a new plate, for LDH measurements after the full kill. The collected medium was mixed with 200 μl of reagent solution containing 0.21 mM NADH, dissolved in LDH buffer (33.3 mM KH_2PO_4 and 66.7 mM $K_2HPO_4 \cdot 3H_2O$, *p*H 7.4). The reaction was started with 25 μl sodium pyruvate (22.7 mM, prepared in LDH buffer) and the kinetic conversion of NADH into NAD^+ was followed for 5 min, at 340 nm, in a microplate reader (Synergy H1, Bio-Tek Instruments). The final volume of reaction in each well was previously set to 275 μl with LDH buffer. Final results of LDH released into the extracellular medium (LDH leakage) were expressed as cell death values calculated as previously described.[26]

K. Statistical analysis

All data are presented as mean + standard deviation (SD), except when stated otherwise, of at least three independent experiments whenever possible. Data were analyzed using GRAPHPAD PRISM software v.6.0 (GraphPad Software, San Diego, CA). Normality of the data distribution was assessed applying three tests: KS normality test, D'Agostino and Pearson omnibus normality test and Shapiro-Wilk normality test. Differences between the average *Tc* were estimated using ordinary two-way analysis of variance (ANOVA) followed by Dunnett's multiple comparisons post-test. In the AnV–FITC/Pi double staining, PrestoBlue and LDH experiments, differences between controls and treatments at each time-point were estimated using ordinary two-way ANOVA followed by Tukey's multiple comparisons test. For the caspase-3 activity experiments, the change of the protein corrected-fluorescence signal with incubation time (RFU μg^{-1} min^{-1}) was determined by linear regression analysis for each control or treatment and plotted as caspase-3 activity values. Differences in caspase-3 activity values were estimated using one-way ANOVA (Kruskal-Wallis) followed by Dunn's multiple comparisons test. P values under 0.05 were considered statistically significant.

III. RESULTS AND DISCUSSION

A. Two nanoparticle populations

The two independent particle populations of our MHT strategy were implemented by design to have specific (targeted) and nonspecific (nontargeted) interactions with cancer cells. For the specifically interacting population, we functionalized protein-A-modified 250-nm magnetic particles (MP) with an anti-CXCR4 antibody (MP–CXCR4) that is able to recognize and target the highly overexpressed (compared to normal, freshly isolated PBMC) CXCR4 receptor in Jurkat (JK) cells [Fig. 1(a)]. Although some nonspecific retention of those particles was observed, the surface targeting of JK cells with the CXCR4 functionalized particles (JK+MP–CXCR4) was confirmed by flow cytometry and LSCM, whereby antibodies attached to the MPs were labeled with fluorescent secondary antibodies [Figs. 1(b) and 1(c)].

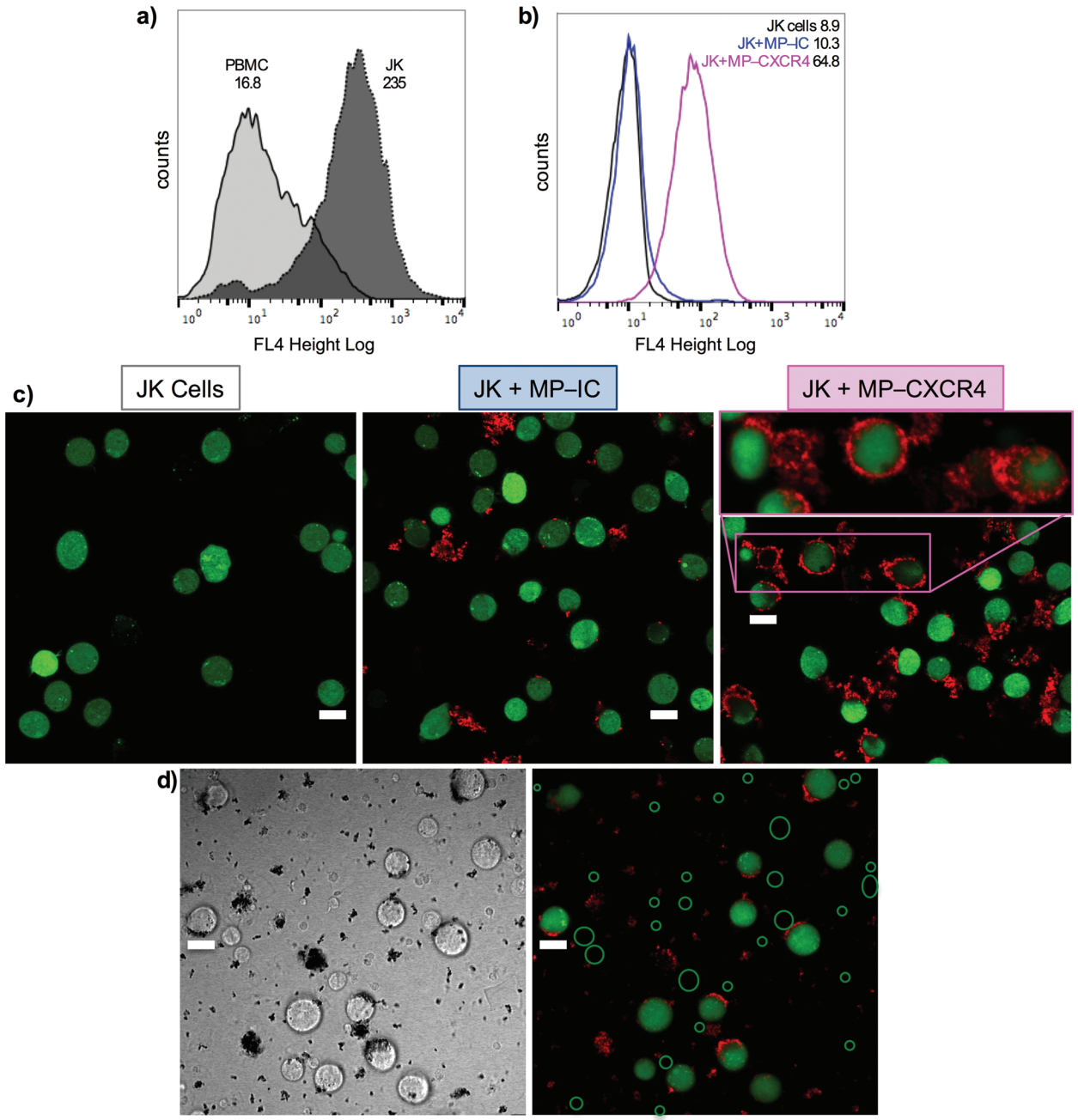

FIG. 1. Studying the interaction between MPs and cells. (a) Differences in surface expression of CXCR4 between JK and PBMC. JK express more than 10× higher levels of that surface receptor than normal PBMC. JK cells labeled with calcein-AM were incubated with IC- or CXCR4-targeted particles and analyzed using (b) flow cytometry and (c) laser scanning confocal fluorescence microscopy (LSCM). A fluorescently labeled secondary antibody (atto-633 IgG) was used to detect the antibodies attached to the particles. Flow cytometry measurements (b) show an increase in the mean fluorescence intensity emitted by JK cells (selected as calcein-positive events) on the atto-633 detection channel (FL4) when using CXCR4-targeted particles, indicating that these particles are recognizing and binding to these cells. The numbers in the graph correspond to the mean fluorescence intensity values of the respective conditions. These results were further confirmed by LSCM (c), which showed JK cells (staining green) surrounded by CXCR4-targeted particles (staining red, right panel). The inset shows a zoomed 3D detail of the selected area. (d) Bright-field and LSCM images of CXCR4-targeted MPs (red) in a mixture of calcein-labeled JK cells (full green) and unlabeled isolated PBMC (marked as green empty circles in the fluorescence image), prepared as described in the supplementary material (Ref. 42), denoting the preferential binding of CXCR4-targeted MPs to JK cells. Scale bars = 10 μm.

Both techniques showed increased fluorescence in cells targeted with MP–CXCR4 in comparison to cells only (JK) and cells with MP–IC (MPs functionalized with an IC antibody). The complex 3D microstructures formed by agglomerates of fluorescently labeled MP–CXCR4 particles around the JK cells are highlighted in the 3D view inset [Fig. 1(c), right panel]. Furthermore, these CXCR4-targeted MPs could recognize and preferentially bind to JK cells within a mixed sample of calcein-labeled JK and freshly isolated PBMC [Figs. 1(d) and S1 in supplementary material[42]], in line with the more than 10× higher CXCR4 expression in JK cells compared to PBMC [Fig. 1(a)].

TABLE I. Iron quantification by inductively coupled plasma–optical emission spectrometry.

Sample	Initial iron ($g_{Fe}\,l^{-1}$)	Iron per sample ($g_{Fe}\,l^{-1}$)	pg Fe per cell	% particle retention[a]
JK+SPION	0.362	0.009 ± 0.004	4.3 ± 2.1	2.4
JK+MP–CXCR4	0.396	0.244 ± 0.025	122.0 ± 12.7	61.6
JK+SPION+MP–CXCR4	0.362 + 0.396	0.309 ± 0.004	154.5 ± 2.1	40.8
JK+SPION+MP–IC	0.362 + 0.396	0.168 ± 0.021	84.0 ± 10.6	22.2

[a]The percentage of particle retention was calculated as 100× ratio between the average iron per sample and the initial iron concentration, for each sample (cumulative for the experiments using two nanoparticle populations). Results are mean ± SD of two independent experiments.

This targeted association of MP–CXCR4 particles with JK cells was further corroborated by ICP-OES results (Table I) that showed retention of 61.6% of the MP–CXCR4 particles by JK cells after incubation followed by the removal of free particles.

Unlike the specific MP–CXCR4 particles, only 2.4% of the nonspecific SPIONs became associated with JK cells after incubation followed by the removal of free particles (Table I). This modest uptake is corroborated by transmission electron microcopy (TEM) imaging that shows only a minimal number of SPIONs associated with the cell membrane (Fig. 2, solid arrows), in contrast to the extensive adsorption and agglomeration of MP–CXCR4 particles at JK cell surfaces [Fig. 1(c), right panel]. Uptake of some SPIONs into endosomal compartments in JK cells is also evident in the TEM image (Fig. 2, hollow arrow).

When using two nanoparticle populations for MHT, the incubation procedure involved four sequential steps: first, a 2-h incubation of cells with SPIONs (0.362 $g_{Fe}\,l^{-1}$); second, removing the excess of free SPIONs; third, a 1-h incubation with MP–CXCR4 (0.396 $g_{Fe}\,l^{-1}$); and fourth, removing the excess of free MPs. Removing the excess of free particles after each incubation step ensures a realistic *in vitro* assessment of volumetric MHT effectiveness that includes only the contribution from the particles associated with the cells. To account for the removed free particles, the representative iron concentration for our MHT experiments was measured by ICP-OES and calculated to be 0.309 $g_{Fe}\,l^{-1}$ (≈5.5 mM) in the JK+SPION+MP–CXCR4 samples and 0.168 $g_{Fe}\,l^{-1}$ (≈3.0 mM) in the JK+SPION+MP–IC samples (Table I). This represents more than 40 and 20%, respectively, of the total initial iron amount these samples were exposed to (0.758 $g_{Fe}\,l^{-1}$ ≈ 13.5 mM, Table I).

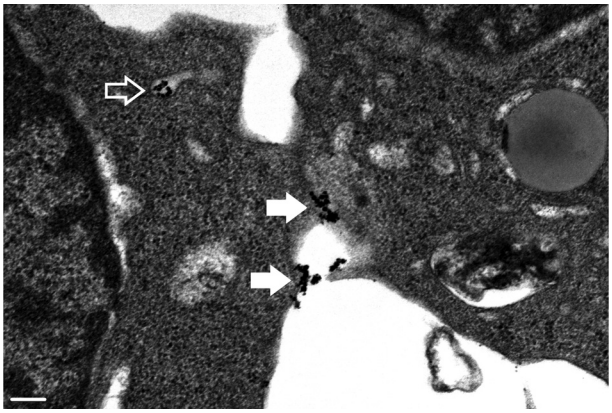

FIG. 2. Interactions between SPIONs and cells. TEM micrograph showing JK cells with SPIONs internalized in endosomal compartments (hollow arrow) or interacting with the cell membrane (solid arrows). Scale bar = 200 nm.

Interestingly, and in agreement with previous reports,[27,28] using flow cytometry, we observed changes in the internal complexity (side-scatter signal) of the cells incubated with nanoparticles, further complementing the data supporting the interaction between cells and nanoparticles (Fig. S2 in the supplementary material[42]).

B. MHT treatment

After optimization of the AMF parameters (Figs. S3 and S4 in the supplementary material[42]), the heating profile in our experiments matched that recommended in a recent review for optimal MHT.[29] The optimized AMF profile was applied to cells with or without nanoparticles following a two-step process, whereby temperature mainly rises during the first AMF step (30 min, 869 kHz, 20 kA m^{-1}) (T_{inc}) and stabilizes in the second AMF step (30 min, 554 kHz, 24 kA m^{-1}) at an average constant temperature (Tc) that depends on the particles used and their functionalization (Fig. 3).

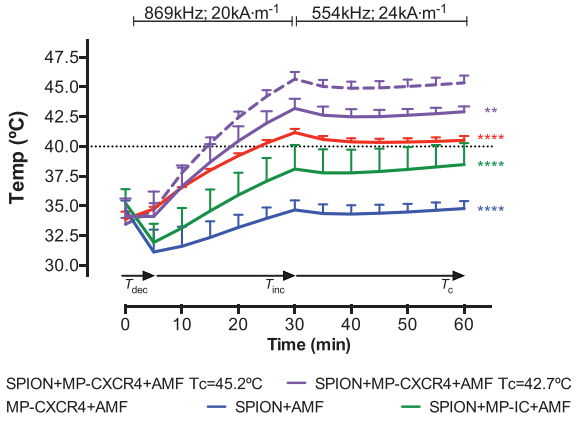

FIG. 3. Heating profiles of JK cells incubated with SPIONs and/or antibody-functionalized MPs. The samples were exposed to an AMF for 1 h, until a Tc was reached. The graph shows an initial sample cooling (T_{dec}) due to the lack of thermal insulation, followed by a temperature increase (T_{inc}), and a final stabilization phase for the last 30 min of MHT (Tc). When a combination of SPIONs and CXCR4-functionalized MPs were used, average Tc of 42.7 or 45.2 °C were observed. The curves represent the mean + SD of two (MP-CXCR4+AMF), three (SPION+AMF) or four (all other conditions) independent experiments. Differences between the average Tc values were estimated using ordinary two-way ANOVA followed by Dunnett's multiple comparisons test. $^{**}p < 0.01$, $^{****}p < 0.0001$ vs JK + SPION + MP − CXCR4 + AMF Tc = 45.2 °C.

A minor artifact related to a limitation of our equipment, during the initial phase, a decrease of temperature can be observed for all samples (T_{dec}), due to the time needed for the heating to be effective after placing the samples, which were preincubated at 37 °C, inside the coil. This artifact would not be applicable in a living organism.

For each particle population independently, the *T*c reached under AMF was relatively low: 34.5 °C for the JK+SPIONs and 40.5 °C for the JK+MP–CXCR4 samples (Fig. 3). The MHT did not induce perceptible cytotoxicity in the presence of SPIONs alone (Fig. S5 in the supplementary material[42]). The higher *T*c reached for JK+MP–CXCR4 samples led to a significant increase of caspase-3 activity; however, it did not produce a significant effect on viability of targeted cells (Fig. S5 in the supplementary material[42]). Given the >60% retention of the MP–CXCR4 particles by JK cells (Table I), further optimization of the targeting is unlikely to increase the iron loading from MP–CXCR4 particles alone to produce significant cytotoxicity in targeted cells. Notably, simple optimization strategies for increasing the targeted MP loading (on a volumetric or per cell basis), such as increasing the cell concentration or performing sequential incubations with targeted MPs, did not result in significant increases in *T*c (data not shown). Conversely, supplementing the specific MP–CXCR4 with a second (nonspecific) SPION population opens the possibility for a more substantial increase in iron loading and the associated effectiveness of MHT. The high SAR of our SPIONs (261 W g^{-1} vs 220 W g^{-1} for MP–CXCR4 particles), under the AMF conditions used in this work, further supports the practicality of the two-population strategy.

C. MHT treatment outcome—Apoptosis versus necrosis

Serendipitously, after MHT experiments, we observed both apoptotic and necrotic outcomes that strongly correlated with the average reached *T*c: 42.7 and 45.2 °C, respectively (Fig. 3, purple curves). In the first outcome group ($n = 4$, $Tc = 42.7$ °C), the cell death pathway appears to be predominantly apoptotic, with a discrete increase in the number of AnV^+ cells [Figs. 4(a) and 4(b)] but an evident induction of caspase-3 activity [Fig. 4(c), $p < 0.05$]. The positive control for an apoptotic cell death, STS, clearly increased the number of AnV^+ cells, representing the apoptotic pathway (Fig. 4), as previously described.[30]

In the second outcome group, for which *T*c reached 45.2 °C ($n = 4$), a more destructive scenario was observed, as illustrated in Fig. 4(b) by representative plots of AnV and Pi double staining to study apoptosis. In this outcome group, nearly 60% of the cells stained either Pi, or Pi and AnV double positive, as early as 2 h after MHT [Figs. 4(a) and 4(b)], indicating cell membrane damage, i.e., cell death. These results, along with the lack of caspase-3 activation [Fig. 4(c)], are indicative of a necrotic pathway for cell death. Furthermore, cell viability dropped to zero in these samples 72 h after MHT [Fig. 5(a)], demonstrating the high effectiveness of the treatment.

Notably, when an apoptotic pathway was activated (i.e., JK+STS and JK+SPION+MP–CXCR4+AMF $Tc = 42.7$ °C samples) a slightly different outcome was registered, as the drop in cell viability was significant but not complete. This observation of a more efficient lethal outcome in necrotic versus apoptotic pathway is in agreement with previous conclusions about insufficient effectiveness of apoptotic MHT.[31] Furthermore, induction of necrosis has been proposed[32] as a means to overcome the frequent tumor recurrence observed after cancer treatment with apoptosis-inducing agents, including temperature.[32,33]

Observing different outcomes under identical initial conditions may seem counterintuitive, however, as previously reported,[34] the natural variability of the cell-nanoparticle system can lead to different plateau temperatures. This natural variability highlights a speculative advantage of using two independent particle populations, whereby insufficient specific iron loading could be augmented by the nonspecific population as necessary.

As expected, the cytotoxic effects of MHT were observed only after cells were treated with a combination of both nanoparticle populations (Figs. 4 and 5). This exclusive attribution is supported by the absence of significant cytotoxicity in all negative controls: whenever AMF was not applied (JK+SPION+MP–IC and JK+SPION+MP–CXCR4 samples) or the matched isotype-control antibody was used (JK+SPION+MP–IC+AMF samples). In particular, no significant effects on cell viability were observed in all the negative controls that included only one type of nanoparticles (Fig. S5 in the supplementary material[42]). Given the complexity of the samples systematically compared in these measurements, we have to evaluate the results based on the aggregate characteristics, such as heating curves, *T*c values, and cell-death outcomes.

D. Comparative MHT effectiveness

Notwithstanding the variety of criteria to evaluate the practicality and effectiveness of the proposed MHT strategy, we will focus on the cytotoxic effectiveness of the different MHT treatments rather than on direct comparison of the experimental parameters such as field conditions or particle concentrations. Such direct comparison is hampered by wide variations of the experimental parameters reported in previous MHT studies. For example, while most of the *in vitro* studies use suspended cells from adherent cell lines,[5–8] we chose a suspension cell line as an inherently more appropriate model for testing a volumetric hyperthermia methodology.

We find that our treatment compares very favorably to those reported in the literature. For example, *in vitro* magnetic hyperthermia studies using CREKA-functionalized magnetic nanoparticles reported a 60% decrease in cell viability under AMF conditions similar to ours.[5] Considering the required iron concentration in both provides an insightful

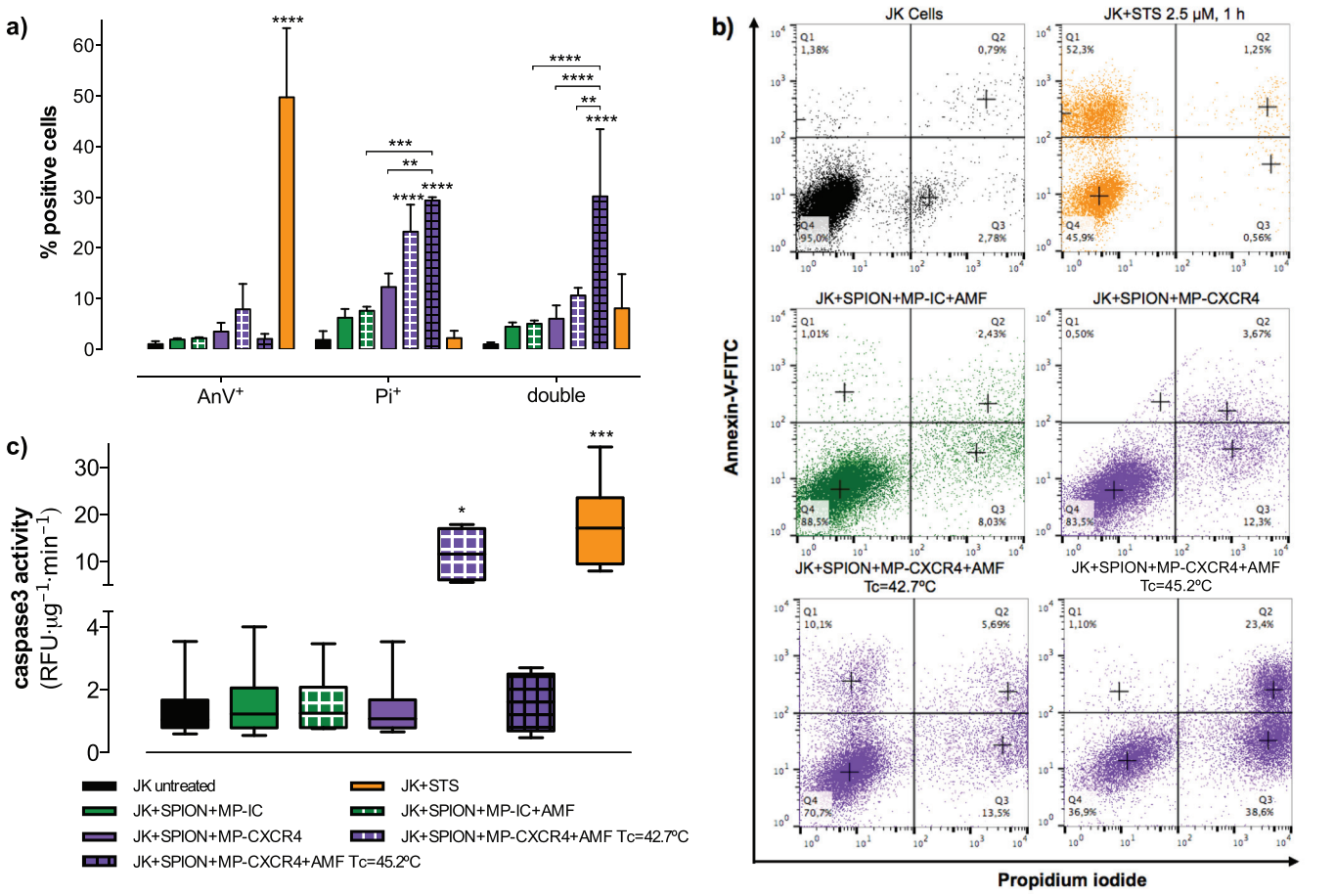

FIG. 4. Apoptosis-induction studies after MHT. (a) and (b) Incubation with AnV–FITC and Pi dyes was performed 2 h after AMF application. The percentage of cells staining positive for each dye individually or together are shown for each treatment/control. A significant increase in Pi^+ cells was observed in JK+SPION+MP–CXCR4+AMF samples, compared to all tested controls, independently of the average reached *T*c. When an average *T*c of 45.2 °C was reached, a significant increase in the double stained events was also observed, showing a total of around 60% dead cells, as early as 2 h after MHT. STS induced a significant increase in the percentage of AnV^+ cells, as expected in an apoptotic cell death pathway. Values are mean + SD of at least three independent experiments. Differences were estimated using one-way ANOVA (Kruskal-Wallis) followed by Dunn's multiple comparisons test. (c) An induction of caspase-3 activity was observed in JK+SPION+MP–CXCR4+AMF samples when *T*c was 42.7 °C and in the tested positive control for apoptosis (STS). Values are min to max with a line at the mean value. Differences between each treatment and untreated control were estimated using one-way ANOVA (Kruskal-Wallis) followed by Dunn's multiple comparisons test. *$p < 0.05$; **$p < 0.01$, ***$p < 0.001$, and ****$p < 0.0001$ vs untreated cells or vs the referred control.

comparative context. In our work AMF is applied after removing the excess free particles that are not associated with the cells. We note that in Ref. 5 AMF was applied without removing the excess free particles and thus the total iron concentration was more than 7× higher than that used in our work (2.2 vs 0.3 $g_{Fe}\,l^{-1}$, respectively). Other studies using functionalized MNPs observed similar MHT effectiveness outcomes; however, a quantitative comparison in terms of iron concentration is not possible because only overall mass-concentration of nanoparticles was reported.[6,7]

In an example using nontargeted nanoparticles, Guardia and coauthors reported a 50%–100% decrease in cell viability *in vitro* in an experiment using magnetic nanocubes.[34] The heating power provides an important basis for the comparison of different AMF protocols for MHT. Specifically, the heating power is an increasing function of the product of the field amplitude *H* and the frequency *f* (*H*·*f* product), which therefore provides a quantitative index of the heating power for a given AMF protocol. In terms of the overall heating efficiency, in both Ref. 34 and our work, samples reached 43 °C after 1 h of AMF exposure. This suggests an approximately linear effect of both AMF power and iron concentration on the heating efficiency, as we used 8× higher *H*·*f* product (the maximum of 17.4×10^9 vs $2.2 \times 10^9\ A\,m^{-1}\,s^{-1}$) and a 6.5–13× lower iron concentration (0.3 vs 2.0–4.0 $g_{Fe}\,l^{-1}$, respectively) to achieve a similar *T*c. In terms of the cell death outcome, in our strategy decreasing cell viability from ca. 15% to ca. 0% (72 h after MHT) required an increase of temperature of only 2.5 °C, whereas with magnetic nanocubes a temperature increase of 22 °C (up to 65 °C), and a concomitant increase in iron concentration to 5 $g_{Fe}\,L^{-1}$ (16× higher than the one used in this work), was reported for reaching 100% cell death.[34] In our approach, a shorter incubation time (3 h vs 24 h) was

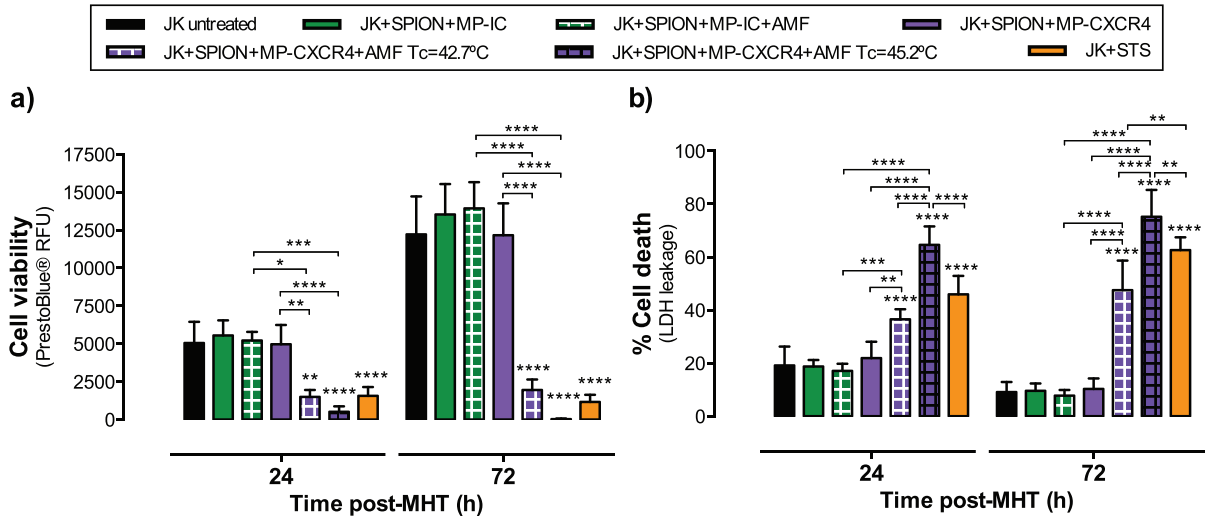

FIG. 5. Cell viability and cell death rates after AMF application. (a) PrestoBlue reagent was used to measure cellular metabolic activity after AMF application, and the emitted fluorescence was compared as a measure of cell viability. Clearly, significant differences in cell viability were observed for the JK+SPION+MP–CXCR4+AMF samples when compared to all the tested controls, in both studied time-points (24 and 72 h post-MHT), and independently of the reached *T*c. Cell viability values after 72 h drastically dropped to zero when the highest *T*c was achieved. (b) Accordingly, the LDH leakage assay results showed a significant increase in cell death levels in JK+SPION+MP–CXCR4+AMF samples. Results are mean + SD of at least four independent experiments performed in triplicate. Differences were estimated using ordinary two-way ANOVA, followed by Tukey's multiple comparison post-test. $*p < 0.05$; $**p < 0.01$; $***p < 0.001$; and $****p < 0.0001$ vs untreated cells or vs the referred sample.

sufficient to reach this outcome. Another previous study that reported SAR values comparable to ours while using AMF with a lower $H{\cdot}f$ product similarly relied on a proportionally higher total iron concentration.[35]

We find the outlook for our strategy of combining specific and nonspecific populations of nanoparticles for MHT to be promising both in terms of effectiveness and the potential range of applications. As discussed earlier, the effectiveness of MHT achieved in our strategy, evaluated via either heating or cell death outcome, favorably compares to those reported in the literature.[5,34,36] Furthermore, our strategy could enhance other implementations of MNP-based cancer therapies and diagnostics. First, it provides a straightforward approach to reaching cytotoxic MHT whenever specific (targeted) iron content alone is insufficient, particularly in a monotherapeutic regimen. We emphasize that the apparent practical limit on the effectiveness of MHT with a single population of targeted MNPs is routinely encountered regardless of the targeting mechanism, specificity, or efficiency,[5,7–9] thereby limiting the gains that can be achieved, for example, by optimizing the targeting antibody.[37] Second, it suggests the possibility of a broader (e.g., tissue-wide or even systemic) application of nontargeted nanoparticles,[38] combined with a more localized and/or targeted strategy. Crucially, the localization of cytotoxic MHT under this strategy remains defined by the specific (targeted) particles, i.e., unaffected by the supplemental nonspecific particle population, which could be optimized[38] to have benign/inert structural and physicochemical properties beyond boosting the iron content. Furthermore, a lower (and more easily manageable) concentration of each component would be required, thereby minimizing the accumulation and potential side effects of the nonspecific particle population on normal cells and tissues. Third, our strategy can directly benefit from all the enhancements of MHT that have been proposed in the literature, including a combination of hyperthermia with chemotherapy agents[17–19] or with photothermal therapy (by taking advantage of both magnetic and photothermal properties of iron oxide nanoparticles),[11] or by confining the MHT application region using a static magnetic field.[39] Conversely, our strategy could be also applicable to enhancing the effectiveness of other treatments known to benefit from combination with hyperthermia.[40] Finally, the magnetic properties of the iron oxide nanoparticles used for MHT can also be exploited for magnetic resonance imaging providing a theranostic tool capable of localizing and eliminating cancer cells.[35,41]

IV. SUMMARY AND CONCLUSIONS

In summary, this work describes an *in vitro* magnetic hyperthermia methodology that effectively achieves a complete loss of cell viability of Jurkat cells using a combination of CXCR4-targeted and nontargeted magnetic nanoparticles. As expected in our strategy, this lethal MHT outcome could only be attributed to the combined iron loading resulting from both specific (targeted) and nonspecific (nontargeted) particle populations. These results confirm the initial hypothesis that targeted-MHT effectiveness may be enhanced by a nontargeted boost of magnetic content. This controlled strategy is a rare example of using MHT in a monotherapeutic context to achieve complete cell death after a 1-h exposure to AMF, therefore proving its promise for future *in vivo* evaluations.

ACKNOWLEDGMENTS

The authors acknowledge the Laboratório de Patologia Clínica Hilário de Lima (Unilabs, Braga, PT) for blood

collection and Marta Oliveira for the help with cell culture. V.V.-B. acknowledges Fundação para a Ciência e Tecnologia (FCT, Portugal) for her Ph.D. fellowship (Grant No. SFRH/BD/82556/2011). This work received financial support from Project No. NORTE-01-0145-FEDER-000024, supported by the Norte Portugal Regional Operational Programme (NORTE 2020), under the PORTUGAL 2020 Partnership Agreement, through the European Regional Development Fund (ERDF). B.E. acknowledges the project Nanotechnology Based Functional Solutions (No. NORTE-01-0145-FEDER-000019), supported by the Norte Portugal Regional Operational Programme (No. NORTE2020), under the PORTUGAL 2020 Partnership Agreement, through the European Regional Development Fund (ERDF).

[1]M. Banobre-Lopez, A. Teijeiro, and J. Rivas, Rep. Pract. Oncol. Radiother. **18**, 397 (2013).
[2]B. Hildebrandt, P. Wust, O. Ahlers, A. Dieing, G. Sreenivasa, T. Kerner, R. Felix, and H. Riess, Crit. Rev. Oncol. Hematol. **43**, 33 (2002).
[3]R. T. Gordon, J. R. Hines, and D. Gordon, Med. Hypotheses **5**, 83 (1979).
[4]Y. Rabin, Int. J. Hyperthermia **18**, 194 (2002).
[5]A. M. Kruse, S. A. Meenach, K. W. Anderson, and J. Z. Hilt, Acta Biomater. **10**, 2622 (2014).
[6]S. H. Liao, C. H. Liu, B. P. Bastakoti, N. Suzuki, Y. Chang, Y. Yamauchi, F. H. Lin, and K. C. Wu, Int. J. Nanomed. **10**, 3315 (2015).
[7]S. Sadhasivam, S. Savitha, C. J. Wu, F. H. Lin, and L. Stobinski, Int. J. Pharm. **480**, 8 (2015).
[8]T. Sadhukha, T. S. Wiedmann, and J. Panyam, Biomaterials **34**, 5163 (2013).
[9]J. Zhang, A. H. Dewilde, P. Chinn, A. Foreman, S. Barry, D. Kanne, and S. J. Braunhut, Int. J. Hyperthermia **27**, 682 (2011).
[10]O. K. Arriortua *et al.*, Beilstein J. Nanotechnol. **7**, 1532 (2016).
[11]A. Espinosa, R. Di Corato, J. Kolosnjaj-Tabi, P. Flaud, T. Pellegrino, and C. Wilhelm, ACS Nano **10**, 2436 (2016).
[12]A. Hervault, A. E. Dunn, M. Lim, C. Boyer, D. Mott, S. Maenosono, and N. T. Thanh, Nanoscale **8**, 12152 (2016).
[13]B. P. Shah, N. Pasquale, G. De, T. Tan, J. Ma, and K. B. Lee, ACS Nano **8**, 9379 (2014).
[14]P. T. Yin, B. P. Shah, and K. B. Lee, Small **10**, 4106 (2014).
[15]C. Yuan, Y. An, J. Zhang, H. Li, H. Zhang, L. Wang, and D. Zhang, Nanotechnology **25**, 345101 (2014).
[16]K. Maier-Hauff, F. Ulrich, D. Nestler, H. Niehoff, P. Wust, B. Thiesen, H. Orawa, V. Budach, and A. Jordan, J. Neurooncol. **103**, 317 (2011).
[17]D. H. Kim, Y. Guo, Z. L. Zhang, D. Procissi, J. Nicolai, R. A. Omary, and A. C. Larson, Adv. Healthcare Mater. **3**, 714 (2014).
[18]H. C. Kim, E. Kim, S. W. Jeong, T. L. Ha, S. I. Park, S. G. Lee, S. J. Lee, and S. W. Lee, Nanoscale **7**, 16470 (2015).
[19]C. A. Quinto, P. Mohindra, S. Tong, and G. Bao, Nanoscale **7**, 12728 (2015).
[20]V. Vilas-Boas, R. Silva, A. R. Gaio, A. M. Martins, S. C. Lima, A. Cordeiro-da-Silva, M. de Lourdes Bastos, and F. Remiao, Cytometry A **79**, 912 (2011).
[21]Y. V. Kolen'ko *et al.*, J. Phys. Chem. C **118**, 8691 (2014).
[22]M. Hedayati *et al.*, Nanomedicine **8**, 29 (2013).
[23]S. Fraga *et al.*, J. Appl. Toxicol. **33**, 1111 (2013).
[24]G. Koopman, C. P. Reutelingsperger, G. A. Kuijten, R. M. Keehnen, S. T. Pals, and M. H. van Oers, Blood **84**, 1415 (1994), available at http://www.bloodjournal.org/content/84/5/1415.
[25]M. J. Valente, R. Henrique, V. Vilas-Boas, R. Silva, L. Bastos Mde, F. Carvalho, P. Guedes de Pinho, and M. Carvalho, Arch. Toxicol. **86**, 249 (2012).
[26]D. J. Barbosa, J. P. Capela, R. Silva, V. Vilas-Boas, L. M. Ferreira, P. S. Branco, E. Fernandes, L. Bastos Mde, and F. Carvalho, Arch. Toxicol. **88**, 455 (2014).
[27]A. Muela, D. Munoz, R. Martin-Rodriguez, I. Orue, E. Garaio, A. A. D. de Cerio, J. Alonso, J. A. Garcia, and M. L. Fdez-Gubieda, J. Phys. Chem. C **120**, 24437 (2016).
[28]M. Poirier, J. C. Simard, F. Antoine, and D. Girard, J. Appl. Toxicol. **34**, 404 (2014).
[29]S. Dutz and R. Hergt, Nanotechnology **25**, 452001 (2014).
[30]A. J. Ullal and D. S. Pisetsky, Apoptosis **15**, 586 (2010).
[31]N. Lee, D. Yoo, D. Ling, M. H. Cho, T. Hyeon, and J. Cheon, Chem. Rev. **115**, 10637 (2015).
[32]S. Y. Proskuryakov, A. G. Konoplyannikov, and V. L. Gabai, Exp. Cell Res. **283**, 1 (2003).
[33]S. Toraya-Brown *et al.*, Nanomedicine **10**, 1273 (2014).
[34]P. Guardia, R. Di Corato, L. Lartigue, C. Wilhelm, A. Espinosa, M. Garcia-Hernandez, F. Gazeau, L. Manna, and T. Pellegrino, ACS Nano **6**, 3080 (2012).
[35]K. Hayashi, M. Nakamura, W. Sakamoto, T. Yogo, H. Miki, S. Ozaki, M. Abe, T. Matsumoto, and K. Ishimura, Theranostics **3**, 366 (2013).
[36]A. J. Giustini, R. E. Gottesman, A. A. Petryk, A. M. Rauwerdink, and P. J. Hoopes, Proc SPIE **7901**, 790118 (2011).
[37]F. Baribaud *et al.*, J. Virol. **75**, 8957 (2001).
[38]N. Guldris *et al.*, Bioconjugate Chem. **28**, 362 (2017).
[39]M. Ma, Y. Zhang, X. L. Shen, J. Xie, Y. Li, and N. Gu, Nano Res. **8**, 600 (2015).
[40]M. N. Centelles, M. Wright, W. Gedroyc, and M. Thanou, Pharmacol. Res. **114**, 144 (2016).
[41]X. L. Liu *et al.*, Adv. Healthcare Mater. **5**, 2092 (2016).
[42]See supplementary material at https://doi.org/10.1116/1.5009989 for additional supporting material for this manuscript is available free of charge: PBMC isolation protocol, comparison between JK cells and PBMC concerning CXCR4 targeting, cell–nanoparticle interaction followed by flow cytometry changes in SSC, cytotoxicity induced by using each type of nanoparticles separately, and optimization of AMF parameters.

SUPPLEMENTAL MATERIAL

Combining CXCR4-targeted and non-targeted nanoparticles for effective unassisted *in vitro* magnetic hyperthermia

Vânia Vilas-Boas[a)]

UCIBIO-REQUIMTE, Laboratory of Toxicology, Biological Sciences Department, Faculty of Pharmacy, University of Porto, Rua de Jorge Viterbo Ferreira, 228, 4050–313 Porto, Portugal

International Iberian Nanotechnology Laboratory, Av. Mestre José Veiga, 4715-330 Braga, Portugal

Begoña Espiña, Yury V. Kolen'ko, Manuel Bañobre-Lopez

International Iberian Nanotechnology Laboratory, Av. Mestre José Veiga, 4715-330 Braga, Portugal

José A. Duarte

CIAFEL, Faculty of Sports, University of Porto, Rua Dr. Plácido da Costa 91, 4200-450 Porto, Portugal

Verónica C. Martins[#]

International Iberian Nanotechnology Laboratory, Av. Mestre José Veiga, 4715-330 Braga, Portugal ([#]current address: INESC – Microsistemas e Nanotecnologias, Rua Alves Redol 9, Lisbon 1000-029, Portugal)

Dmitri Petrovykh[a), b)], Paulo P. Freitas

International Iberian Nanotechnology Laboratory, Av. Mestre José Veiga, 4715-330 Braga, Portugal

Felix D. Carvalho[a)]

UCIBIO-REQUIMTE, Laboratory of Toxicology, Biological Sciences Department, Faculty of Pharmacy, University of Porto, Rua de Jorge Viterbo Ferreira, 228, 4050–313 Porto, Portugal

[a)]Electronic mail: vvilasboas@ff.up.pt dmitri.petrovykh@inl.int felixdc@ff.up.pt

[b)]American Vacuum Society member.

A. PBMC isolation

The isolation of mononuclear cells from peripheral blood was performed following a previously established protocol.[Ref 20] Briefly, whole blood from an informed healthy volunteer was collected to EDTA tubes and carefully layered on top of equal volume of Histopaque-1077 (Sigma-Aldrich, Inc., St. Louis, MO, USA) previously equilibrated at room temperature, and immediately centrifuged at 650 *g*, 10 min, at room temperature, in a swing bucket centrifuge. The interface containing mononuclear cells was collected and washed with PBS. The approximate number of PBMC was counted in a Neubauer counting chamber after diluting the sample in Turk solution (Sigma-Aldrich, Inc., St. Louis, MO, USA).

B. Confirming specific (targeted) interactions: Jurkat vs. PBMC

JK cells or freshly isolated PBMC were incubated with calcein-AM 1 μM at 37 ´C and further incubated MP–IC or MP–CXCR4 for 1 h, at 37 ºC. After centrifuging the samples for 5 min at 125 *g*, cells were incubated for 30 min at 37 ºC with the atto-633 labeled secondary antibody. After a last centrifugation step, cells were kept on ice until flow cytometry analysis. Flow cytometry parameters were set as described in "*Confirming specific (targeted) interactions*" section of the main text. Fluorescence due to calcein was followed in FL-1 channel, and the one due to atto-633 was followed on FL-4 channel. Flow cytometry standard files were analyzed using FlowJo v10.1 software.

In accordance with the distinct CXCR4 expression levels (Fig. 1a, main text), more MP–CXCR4 were found interacting with JK cells than with PBMC (Fig. S1). In fact, while only around 20 % of the PBMC were labeled using the CXCR4-targeted

particles (second peak in the PBMC+MP–CXCR4 sample), the JK cells could be fully labeled under similar conditions (100 % of the JK cells shift to the right as JK+MP–CXCR4, compared to JK+MP–IC presented in Fig.1b of the main text). In contrast with JK cells (Fig. 1b and c, main text), we observed some nonspecific retention of the MP–IC in the PBMC samples (asymmetric tail in the blue line, Fig. S1).

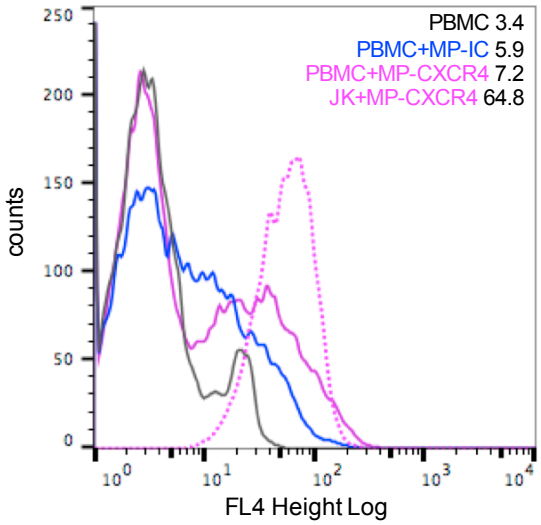

FIG. S1 – Assessing the interaction of MP–CXCR4 with JK cells or PBMC by flow cytometry. Interaction between CXCR4-targeted MPs and both types of cells is clearly distinct, with JK cells carrying more MP–CXCR4 (dashed pink line) than the freshly isolated PBMC (full pink line). Some degree of nonspecific retention of MP–IC in the PBMC samples was observed (asymmetric tail in the blue line).

Flow cytometry data obtained after co-incubation of JK cells and nanoparticles indicate that both particle populations interact with the cells (Fig. S2), showing different light scattering properties (in forward scatter, FSC, and side scatter, SSC, detectors) depending on the type of particles. Figure S2 clearly shows the movement of the gated events up on the SSC-Height axis, related to cell granularity or complexity, from a JK cells-only sample (31.1 ± 4.9) to JK+SPIONs (73.4 ± 0.6), and then to JK+MP–CXCR4

(135.0 ± 7.6). When a combination of both particles was used, features of both scattering patterns of cell-particle events were observed, reaching an intermediate SSC value (90.1 ± 11.8).

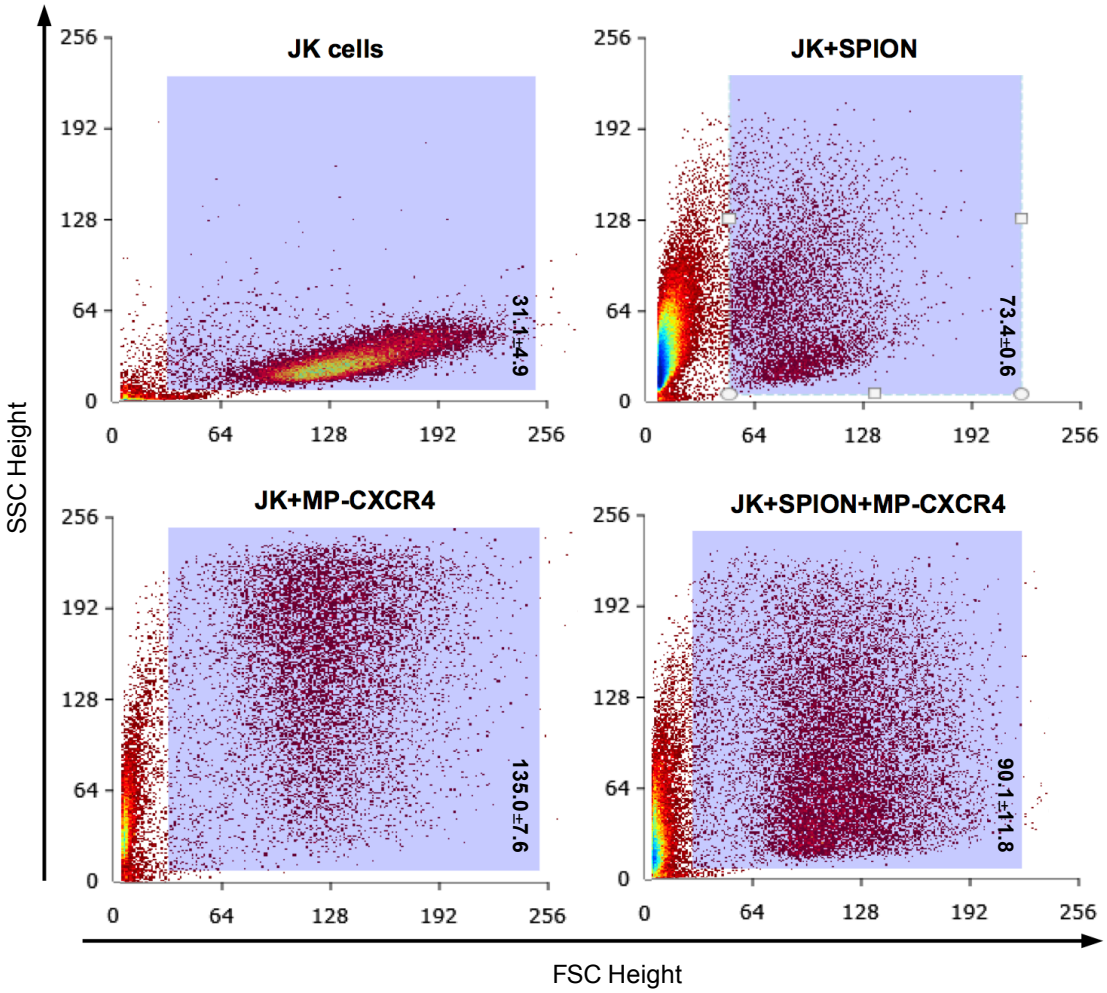

FIG. S2 – Light scattering properties of Jurkat cells incubated with SPION and/or CXCR4-targeted MPs. Flow cytometry data showing changes in light scattering properties due to the presence of different nanoparticles, alone or in combination, an indication of interaction between particles and cells. The mean±SD values from three independent experiments collected by the side scatter detector are presented in each representative dot plot.

C. Optimization of AMF parameters

The MHT experiments were performed using a DM 100 nB nanoScale Biomagnetics AMF applicator equipped with an optical temperature probe. The influence of the different combinations of AMF parameters on cell viability was initially studied in order to select the conditions that would lead to higher MHT efficiency. To do so, U87MG cells (ATCC® HTB-14™, cultivated in a controlled atmosphere containing 5 % CO_2, at 37 ºC, in Eagle's Minimum Essential Medium + 10 % Hyclone FBS) were detached using trypsin, incubated with SPIONs and submitted to different combinations of frequency and field amplitude, as shown in Fig. S3. These preliminary results suggested that submitting the samples to temperatures above 40 ºC for longer periods increased MHT efficiency. Cell viability levels were evaluated immediately after MHT using PrestoBlue® cell viability reagent. These results were further confirmed 24 h after MHT, by laser scanning confocal microscopy, after staining the cell nucleus with Hoechst 33342 (ThermoFisher Scientific) and the dead cells with propidium iodide (Sigma Aldrich).

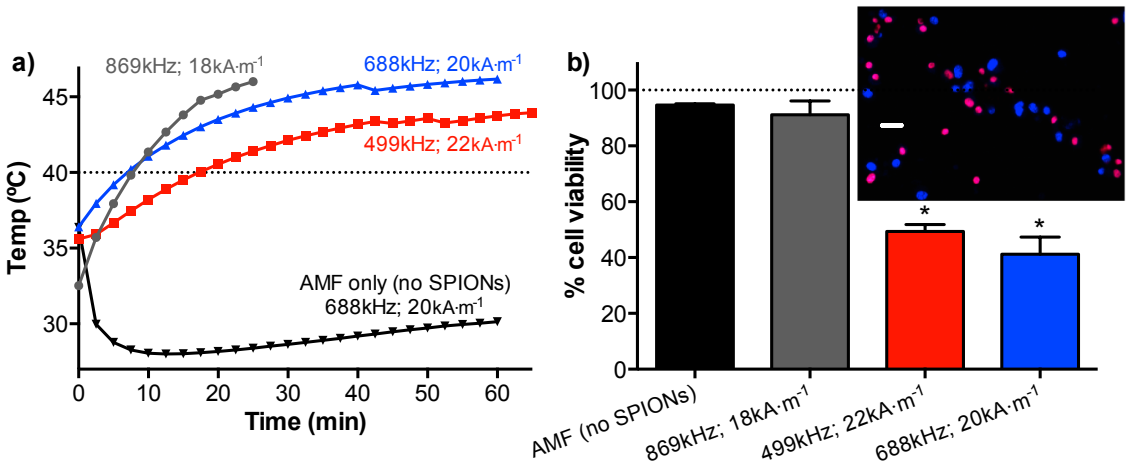

FIG. S3 – Optimization of AMF parameters for efficient MHT. a) Different AMF parameters were tested to evaluate the most efficient MHT conditions to be applied in our study. b) Viability tests immediately after MHT indicate that exposing the samples to temperatures above 40 ºC for longer periods of time (red and blue curves) leads to more significant reductions in cell viability, to less than 50 %. Imaging Hoechst 33342 and PI-labeled cells by laser scanning confocal microscopy 24 h after MHT further confirmed the levels of cell death (inset; scale bar is 20 μm). The AMF (688 kHz, 20 $kA \cdot m^{-1}$) or the SPIONs-only did not significantly impair cell viability. Differences were estimated using one-way ANOVA (Kruskal-Wallis test) followed by a Dunn's multiple comparisons test. ***p<0.001 and ****p<0.0001 *vs.* untreated cells (100 % line in the graph).

Based in the preliminary results reported above, further tests were performed to select the final conditions to be used in the work herein presented. Our *in vitro* model of T-cell leukemia, Jurkat cells (JK), was used for these optimization studies. Two different protocols were established using a two-step procedure: A - 869 kHz, 20 $kA \cdot m^{-1}$, 30 min + 554 kHz, 24 $kA \cdot m^{-1}$, 30 min, or B – 554 kHz, 24 $kA \cdot m^{-1}$, 30 min + 869 kHz, 20 $kA \cdot m^{-1}$, 30 min. Figure S4 shows the heating profiles obtained when applying protocols A or B to JK cells previously incubated for 1 h, with MP–CXCR4, after removing the excess of free MPs by centrifugation (125 *g*, 5 min).

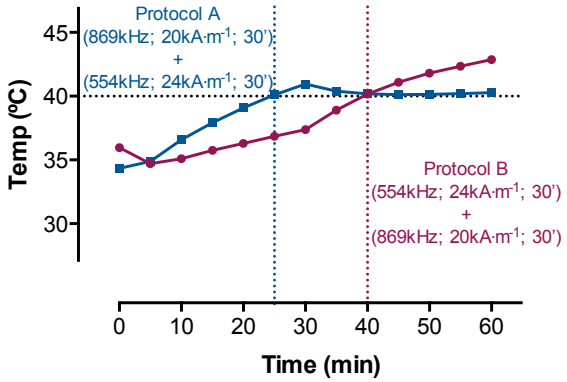

FIG. S4 – Selection of AMF parameters for efficient MHT on Jurkat cells. Two different 1 h AMF protocols were tested: protocol-A – 30 min at 554 kHz, 24 $kA \cdot m^{-1}$, followed by 30 min at 869 kHz, 20 $kA \cdot m^{-1}$; protocol-B – 30 min at 554 kHz, 24 $kA \cdot m^{-1}$, followed by 30 min at 869 kHz, 20 $kA \cdot m^{-1}$. In protocol-A 40 ºC are reached in 25 min and temperature is kept above this level throughout the rest of the protocol. Protocol-B needed more time to reach 40 ºC (40 min), which may limit the exposure time to high and damaging temperature.

The heating curve from protocol-A shows that a high temperature (above 40 ºC) is reached in the first half of the protocol, which is kept in the second half of the AMF application as a consequence of a decrease in the overall AMF power. Following protocol-B, in turn, leads to a lower temperature (than protocol-A) in the end of the first half of the procedure, which further increases in the second half of the protocol due to the overall increase AMF power. Although a higher absolute temperature is reached at the end of protocol-B application, protocol-A reached 40 ºC in 25 min and the temperature was kept above this threshold for efficient MHT for at least 35 min. These findings suggest protocol-A to be the most suitable, amongst the tested, to be applied in the subsequent work.

D. MHT-induced cytotoxicity when using SPION or MP–CXCR4 separately

Figure S5 presents the caspase-3 kinetic assay and cell viability levels for JK cells with each particle population independently, after exposure to the selected AMF conditions (protocol-A, Fig. S4). As stated in the main text, MHT performed on JK+SPION+AMF samples did not produce cytotoxicity signatures. For the JK+MP–

CXCR4+AMF samples, caspase-3 activity was significantly induced ($p<0.001$, Fig. S5) but failed to produce a significant reduction in cell viability levels.

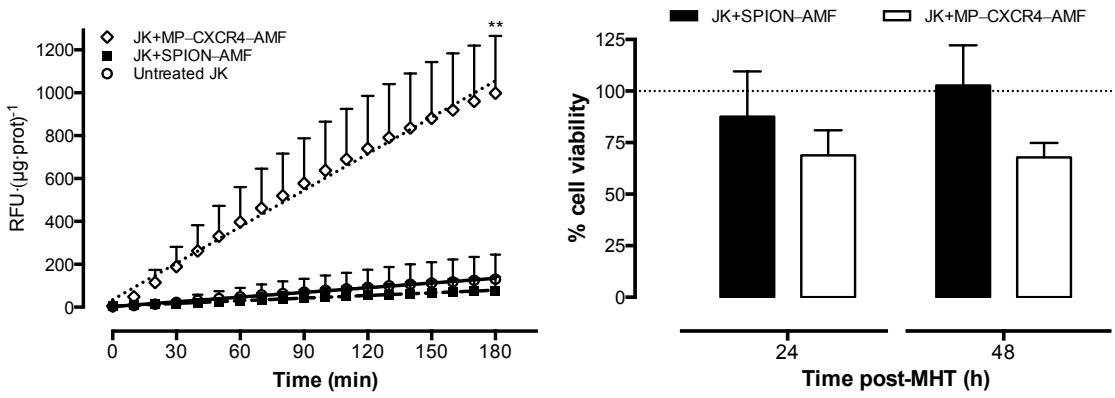

FIG. S5 – Caspase-3 and cell viability assays after MHT application when only one type of particles was used. When using SPIONs only, average *T*c was kept around 34.5 ºC (see Fig. 1 of the main text), which is not expected to affect cell viability. Indeed, caspase-3 activity did not significantly change, and cell viability was not significantly impaired, comparing to cells-only control (100 % dashed line). When using only MP–CXCR4, the average *T*c was 40.5 ºC (see Fig. 1 of the main text), which could yield some toxicity in cancer cells. An evident increase in caspase-3 activity was observed in this case (**$p<0.001$ *vs.* untreated cells), but cell viability did not decrease more than 35 %. Differences between the observed caspase-3 slopes were estimated using repeated measures two-way ANOVA followed by Dunnett's multiple comparisons test; differences between treated and untreated cell viability rates in both time-points were estimated using ordinary two-way ANOVA followed by Dunnett's multiple comparisons test.